Article

Blood Flow and Bmp Signaling Control Endocardial Chamber Morphogenesis

Ann-Christin Dietrich,[1,2,3,4] Verónica A. Lombardo,[1,2,3,4] Justus Veerkamp,[3] Florian Priller,[3] and Salim Abdelilah-Seyfried[1,2,3,*]

[1]Institute of Biochemistry and Biology, University of Potsdam, Karl-Liebknecht-Straße 24-25, 14476 Potsdam, Germany
[2]Institute for Molecular Biology, Medizinische Hochschule Hannover, Carl-Neuberg Straße 1, 30625 Hannover, Germany
[3]Max Delbrück Center for Molecular Medicine, Robert-Rössle Straße 10, 13125 Berlin, Germany
[4]Co-first author
*Correspondence: salim.seyfried@uni-potsdam.de
http://dx.doi.org/10.1016/j.devcel.2014.06.020

SUMMARY

During heart development, the onset of heartbeat and blood flow coincides with a ballooning of the cardiac chambers. Here, we have used the zebrafish as a vertebrate model to characterize chamber ballooning morphogenesis of the endocardium, a specialized population of endothelial cells that line the interior of the heart. By combining functional manipulations, fate mapping studies, and high-resolution imaging, we show that endocardial growth occurs without an influx of external cells. Instead, endocardial cell proliferation is regulated, both by blood flow and by Bmp signaling, in a manner independent of vascular endothelial growth factor (VEGF) signaling. Similar to myocardial cells, endocardial cells obtain distinct chamber-specific and inner- versus outer-curvature-specific surface area sizes. We find that the hemodynamic-sensitive transcription factor Klf2a is involved in regulating endocardial cell morphology. These findings establish the endocardium as the flow-sensitive tissue in the heart with a key role in adapting chamber growth in response to the mechanical stimulus of blood flow.

INTRODUCTION

In zebrafish, the heart forms de novo through an aggregation of cardiomyocytes and tightly associated endocardial progenitor cells at the embryonic midline (reviewed in Staudt and Stainier, 2012). Subsequently, with the onset of blood flow, the two cardiac chambers massively expand in size in a process known as cardiac ballooning (between 30 and 54 hr postfertilization [hpf]). The main mode of myocardial growth during the stages of cardiac ballooning occurs through a continuous accretion of cells at the arterial and venous poles of the heart (de Pater et al., 2009; Hami et al., 2011; Lazic and Scott, 2011; Zhou et al., 2011) rather than through a proliferation of progenitor cells within the heart (Rohr et al., 2006).

Zebrafish cardiac ballooning involves the acquisition of chamber- and region-specific cardiomyocyte morphologies, leading to a characteristic expansion of the outer curvature regions and a compaction of the inner curvature regions of the ventricular chamber. These myocardial shape changes, which play a crucial role in defining cardiac form, have been partially linked to cardiac contractility and to hemodynamic forces within the ballooning heart (Auman et al., 2007). Similarly, the expansion of ventricular cardiomyocyte cell surface area and myofibrillar content has been linked to blood flow (Lin et al., 2012). However, previous studies have failed to address the cellular processes by which endocardial chambers emerge during cardiac ballooning stages, the extent to which the morphogenesis of the endocardium mirrors that of the myocardium, and whether endocardial mechanosensitive responses to blood flow affect endocardial and myocardial cell morphologies.

Genetic evidence suggests that endocardial progenitor cells represent a subset of a larger endothelial progenitor cell pool (Harris and Black, 2010; Puri et al., 1999; Stainier et al., 1995; Staudt and Stainier, 2012). By 48 hpf, the endocardium is organized into arterial and venous subpopulations with comparable gene expression profiles similar to that of the vascular network. For example, arterial endothelial cells and endocardial cells of the ventricular chamber both express *notch1b* at 48 hpf (Vermot et al., 2009), which identifies this subpopulation of endocardial cells as arterial tissue, whereas endocardial cells of the atrial chamber lack expression of this gene. The establishment of chamber-specific expression patterns is impaired in embryos that lack blood flow (Vermot et al., 2009). Although endocardial cells of the two cardiac chambers can be distinguished based on gene expression patterns, it is currently not known whether these populations show distinct cellular behaviors or morphological adaptations.

The growth and remodeling of blood vessels require angiogenesis signaling, which leads to the formation of new blood vessels from preexisting vessels. In most endothelial tissues, angiogenesis signaling involves vascular endothelial growth factors (VEGFs), their respective tyrosine kinase receptors (VEGFRs), and Notch signaling (de Vries et al., 1992; Olsson et al., 2006; Shibuya and Claesson-Welsh, 2006; Herbert and Stainier, 2011). Recently, an alternative VEGF-independent mode of angiogenesis involving Bmp signaling has been described in a subset of zebrafish venous endothelial cells (Kim et al., 2012; Wiley et al., 2011). With the onset of blood flow, angiogenesis signaling is modified in response to hemodynamic forces. During zebrafish aortic arch blood vessel formation, the mechanosensitive transcriptional regulator Krüppel-like factor 2a (Klf2a) indirectly activates VEGF-dependent
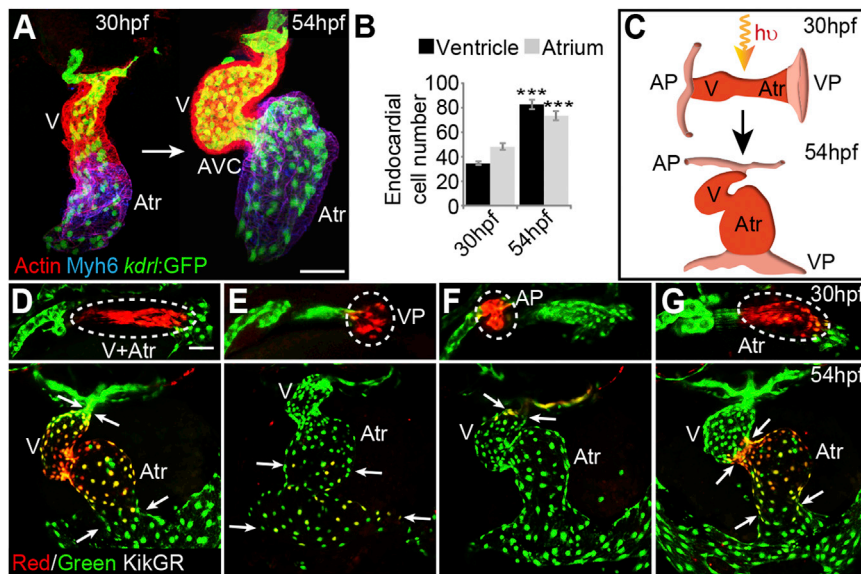
Figure 1. Endocardial Growth during Cardiac Ballooning Occurs without Addition of External Cells

(A and B) Endocardial cell numbers approximately double between heart tube (30 hpf) and ballooning stages (54 hpf; mean with SEM; n ≥ 7 hearts; ***p < 0.001).

(C) Scheme of the photoconversion assays. At the heart tube stage (27–30 hpf), different regions of interest in the endocardium, such as heart tube (ventricle + atrium), arterial pole (AP), venous pole (VP), or atrium (Atr) were photoconverted and analyzed 20 hr later.

(D) Photoconversion of the entire endocardium at 27–30 hpf results in a completely KikGR-red-labeled endocardium at 51–54 hpf. Hence, endocardial progenitor cells present in the heart tube give rise to the endocardial ballooning heart without influx of external cells.

(E) In comparison, photoconverted cells of the venous pole region solely contribute to the inflow region.

(F and G) Photoconverted cells of the arterial pole contribute to the aorta (F), and photoconverted cells of the atrium contribute exclusively to the atrium (G). Each assay was repeated at least three times with invariant results. Dashed lines indicate regions of interest; white arrows demarcate the boundaries of regions with photoconverted cells. Scale bar represents 50 μm.

See also Figures S1 and S2.

angiogenesis signaling (Nicoli et al., 2010). Within blood vessels, the mechanical force of shear stress is a strong inducer of Klf2 (Dekker et al., 2002). The integration of blood flow and angiogenesis signaling links blood vessel patterning with biophysical parameters. To date, however, no genuine morphogenetic factor or pathway has been shown to be essential for early endocardial tissue morphogenesis.

Within the endocardium, Klf2a is involved in a blood flow-dependent morphogenetic process. Endocardial expression of Klf2a is directly dependent on the retrograde flow fraction, which is the fraction of the cardiac cycle during which flow has a reversed orientation (Vermot et al., 2009). Reversible blood flow patterns, which are particularly high at the atrioventricular canal (AVC), induce high levels of Klf2a, which in turn triggers the expression of notch1b and promotes the formation of cardiac valves (Vermot et al., 2009). However, previous studies failed to address whether hemodynamic forces also affect endocardial growth and ballooning morphogenesis of the endocardial chambers.

Here we investigate the cellular mechanisms involved in endocardial chamber morphogenesis. Using a combination of functional and fate mapping studies, we find that endocardial cells proliferate and acquire chamber- and region-specific cellular shapes and surface areas in response to blood flow. This process contributes to endocardial chamber ballooning independently of VEGF-dependent angiogenesis and without the addition of external cells. That myocardial morphology and chamber ballooning are also affected by altered blood flow (Auman et al., 2007; Lin et al., 2012) defines the endocardium as the flow-sensitive cardiac tissue with an important role in cardiac remodeling in response to dynamically changing blood flow conditions. Our findings suggest a crosstalk between endocardium and myocardium during chamber morphogenesis: endocardial chamber morphogenesis is blood flow-sensitive.

This mechanical trigger also affects myocardial chamber morphogenesis. In turn, Bmp signaling from the myocardium affects endocardial proliferation. This dynamic crosstalk between endocardium and myocardium has important implications for our understanding of the morphological changes of the heart during development or under (patho-) physiological conditions.

RESULTS

Endocardial Cell Proliferation without External Cell Addition Contributes to the Ballooning of Endocardial Chambers

Coinciding with the onset of blood flow, the shape of the zebrafish heart dramatically changes from a narrow linear tube at 30 hpf to a ballooning shape at 54 hpf with two morphologically distinct cardiac chambers: a smaller, muscular ventricle and a larger, thin-walled atrium (Figure 1A). The latter stage is also characterized by a constriction and formation of cardiac cushions at the atrioventricular canal (AVC), which is the boundary between the two chambers (Figure 1A). Because myocardial cells are not proliferative at these developmental stages, the massive increase in cardiac size is mainly driven by the addition of secondary heart field-derived myocardial progenitor cells at both poles of the growing heart (de Pater et al., 2009; Hami et al., 2011; Lazic and Scott, 2011; Zhou et al., 2011).

To determine whether the massive growth of the zebrafish heart during ballooning stages also involves an increase in endocardial cell numbers, we used the transgenic endothelial reporter line Tg(kdrl:EGFP)^{s843}, which labels endocardial cell nuclei, for quantifications (Figure 1A). The two endocardial chambers were identified by counterlabeling the myocardium with an antibody against Myosin, heavy polypeptide 6, cardiac muscle, alpha (Myh6; which marks the atrium), and with rhodamine-phalloidin, which labels Actin within the entire myocardium

(Figure 1A). The AVC region of the endocardium is a specialized region at the boundary between both chambers that is not present at 30 hpf; by 54 hpf, it has become both morphologically and molecularly different from the two chambers. To exclude AVC endocardial cells from chamber endocardial cells during quantifications, we recognized AVC cells based on their characteristic cuboidal morphologies, which was confirmed by immunolabeling against the activated leukocyte cell adhesion molecule (Alcam), a specific marker of the AVC endocardium at this later stage (Figure S1 available online; Beis et al., 2005). Between these two stages, the number of endocardial cells in each chamber approximately doubled (Figure 1B). More precise developmental staging revealed that the endocardial growth of both chambers occurs continuously throughout the entire period (Figure S2A).

Endocardial growth could be due to a proliferation of endocardial progenitor cells confined within the nascent cardiac tube or, alternatively, to the addition of endocardial cells from an external source, similar to the process of myocardial growth. We performed cell lineage tracing studies to distinguish between these possibilities by using the transgenic line Tg(kdrl:nlsKikGR)^{hsc7} (Lazic and Scott, 2011), which expresses the photoconvertible fluorescent protein Kikume green red (KikGR) within all endothelial tissues including the endocardium. The exposure of KikGR to UV or blue light results in a permanent and irreversible fluorescence conversion of the protein into the red color range. The development of cells marked by this stable photoconversion can be followed in the zebrafish embryo (Lazic and Scott, 2011; Lombardo et al., 2012). First, we tested whether endocardial cells that originate outside the nascent heart tube are added to the growing heart between 27 and 54 hpf. To this end, all endocardial cells confined within both cardiac chambers of the 27–30 hpf primary heart tube were labeled by KikGR photoconversion, resulting in an almost complete marking of the endocardium by photoconverted red KikGR positive cells at 51–54 hpf (Figures 1C and 1D; Figure S2B). We identified on average only five unlabeled endocardial cells per heart (total of four hearts). This finding suggested that most endocardial progenitor cells are confined within the 27 hpf primary heart tube as it develops. To further confirm this result, we tested whether venous pole endothelium (Figure 1E; Figure S2C) or arterial pole endothelium (Figure 1F; Figure S2D) contributes to the increase in endocardial cell numbers. We found that these cells were not involved in endocardial growth between 27 and 54 hpf. Finally, we tested whether endocardial cells of the primary heart tube are chamber-restricted by stably photoconverting KikGR only within the future atrium of the 27–30 hpf primary heart tube. We found that this population of cells exclusively contributed to the 51–54 hpf atrial endocardium (Figure 1G; Figure S2E). Hence, endocardial progenitor cells are chamber-restricted and do not cross chamber boundaries between 27 hpf (cardiac tube stage) and 54 hpf (end stages of cardiac ballooning).

We next assayed whether all or just a subset of endocardial cells were proliferative using bromodeoxyurindine (BrdU) pulse labeling with a long incubation period between 24 and 48 hpf. Subsequent staining with an anti-BrdU antibody revealed that all endocardial cells within the heart tube had undergone DNA replication during this incubation period (Figures S2F–S2H).

Taken together, these findings indicate that a high proportion of endocardial progenitor cells are proliferative during cardiac ballooning stages. In addition, growth of the early zebrafish endocardium between 27 and 54 hpf is largely determined by proliferation of endocardial progenitor cells that remain within their original chambers of the nascent heart tube and that any entry of cells from external tissues is insignificant. This process strikingly contrasts myocardial growth, which mostly involves an accretion at both poles of the heart of cells that are derived from extracardiac progenitors.

Endocardial Proliferation Does Not Involve VEGF-Dependent Angiogenesis Signaling during Cardiac Ballooning Stages

VEGF-dependent angiogenesis may be an important pathway for endocardial growth and expansion. The expression of VEGFRs has previously been described in the endocardium (Bussmann et al., 2007) and the predominant proangiogenic ligand VEGFaa is expressed within the anterior vasculature and endoderm close to the cardiac field (Alt et al., 2006). Based on its essential role during vascular development and remodeling, we asked whether this signaling pathway is involved in endocardial growth during cardiac ballooning stages and used the pharmacological VEGFR inhibitor Vatalanib (PTK787) for functional studies (Chan et al., 2002). To depict endocardial and myocardial morphology, we used the endothelial reporter line Tg(kdrl:EGFP)^{s843} (Figures 2A and 2B) or the general myocardial reporter line Tg(myl7:EGFP)^{twu34} (Figures 2C and 2D). Unexpectedly, incubation of embryos with 5–20 μM PTK787 throughout cardiac ballooning stages (24–54 hpf) did not affect endocardial or myocardial chamber morphology (Figures 2B and 2D), cell numbers (Figure 2E), or the ventricle-restricted expression of Tg(flt1:YFP)^{hu4624}, which we found restricted to the ventricle at 54 hpf (Figures 2F and 2G). Intersegmental vessel formation was completely blocked by PTK787 treatment, which confirmed the bioactivity of this inhibitor at that concentration (Figures 2H and 2I; Chan et al., 2002). Taken together, our results show that the growth of the endocardium during cardiac ballooning stages is not regulated by VEGF signaling.

Blood Flow Controls Endocardial Cell Number during Cardiac Ballooning

Because endocardial cell proliferation and endocardial chamber expansion coincides with the onset of circulation, we next tested whether biophysical forces exerted by blood flow are involved in the control of endocardial cell number and chamber ballooning. We investigated this question using three principle methods to modulate hemodynamic forces. First, we analyzed troponinT2a (tnnt2a)^{b109} mutants, which completely lack blood flow due to the absence of an essential sarcomeric protein that is required for cardiac contractility (Sehnert et al., 2002). Second, we altered blood viscosity and shear stress by lowering the hematocrit through knockdown of gata1 and gata2, two genes required for hematopoiesis in zebrafish (Galloway et al., 2005). Embryos injected with gata1;gata2 antisense oligonucleotide morpholinos (MOs), lack all circulating red blood cells and have a strongly reduced blood viscosity and shear stress. Vermot and colleagues measured a reduction of blood viscosity by > 90% using the combination of these MOs (Vermot et al., 2009). Third, we
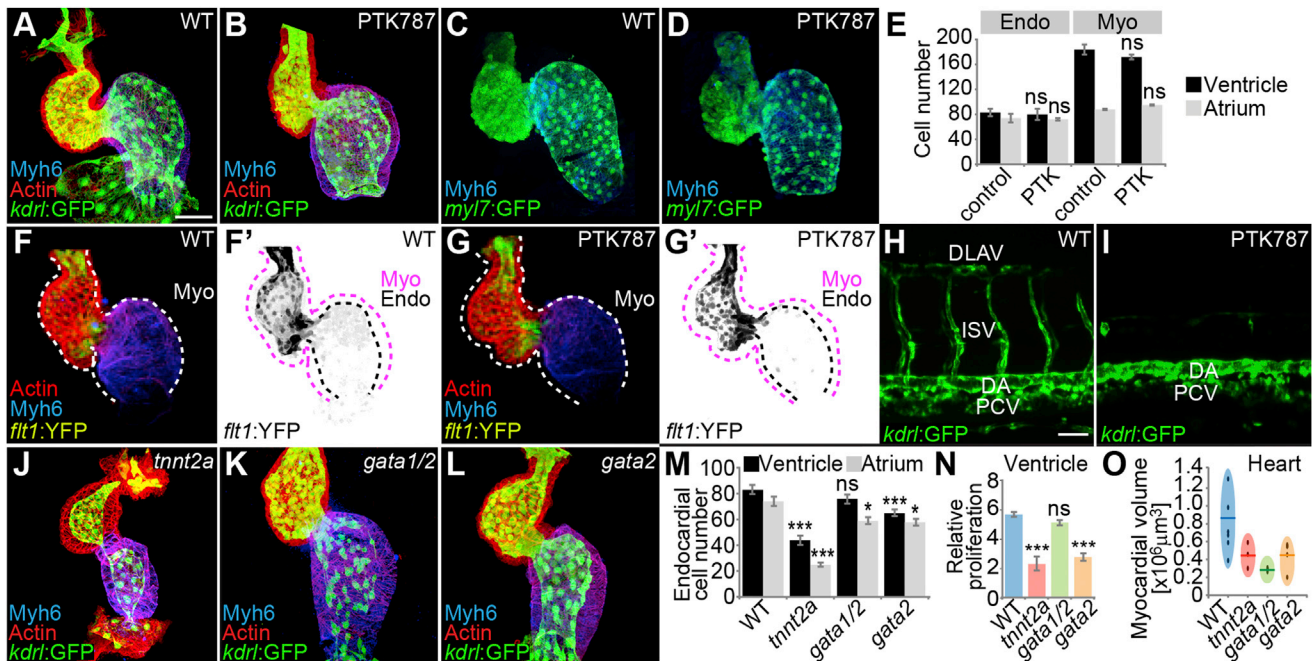
Figure 2. Blood Flow Controls Endocardial Cell Number Independently of VEGF-Dependent Signaling

(A–E) Treatment with the pharmacological VEGFR inhibitor PTK787 (5 μM) throughout cardiac ballooning stages (24–54 hpf) does not affect (B) endocardial and (D) myocardial morphology, or (E) cell number. Quantifications of endocardial cell numbers (mean with SEM; n ≥ 3 hearts per condition; ns, not significant).

(F and G) Inhibition of VEGF-dependent signaling does not affect myocardial chamber-specific marker expression (myocardium is marked with dashed lines) or (G′) endocardial ventricular-restricted expression of VEGFR1 (Flt1; false-colored in black; myocardium is marked with pink dashed lines).

(H and I) Intersegmental vessel (ISV) formation is blocked by 5 μM PTK787 treatment between 24 and 54 hpf. DA, dorsal aorta; DLAV, dorsal longitudinal anastomotic vessel; PCV, posterior cardinal vein.

(J–M) Blood flow controls endocardial cell number during cardiac ballooning stages. (J) Endocardial morphologies under no-blood-flow condition (*tnnt2a*[b109]), (K) reduced shear stress (*gata1/2* morphant), or (L) reduced retrograde flow fraction and shear stress (*gata2* morphant). (M) Quantifications of endocardial cell numbers (mean with SEM; n ≥ 5 hearts per condition; ***p < 0.001, *p < 0.05, ns, not significant).

(N) Relative proliferation rate within ventricular endocardium between 30 and 54 hpf (mean with SEM; n ≥ 5 hearts per condition; ***p < 0.001, ns, not significant).

(O) Measurements of myocardial volume (n ≥ 4 hearts per condition). Each black dot represents an individual heart; lines represent mean values. Scale bar represents 50 μM.
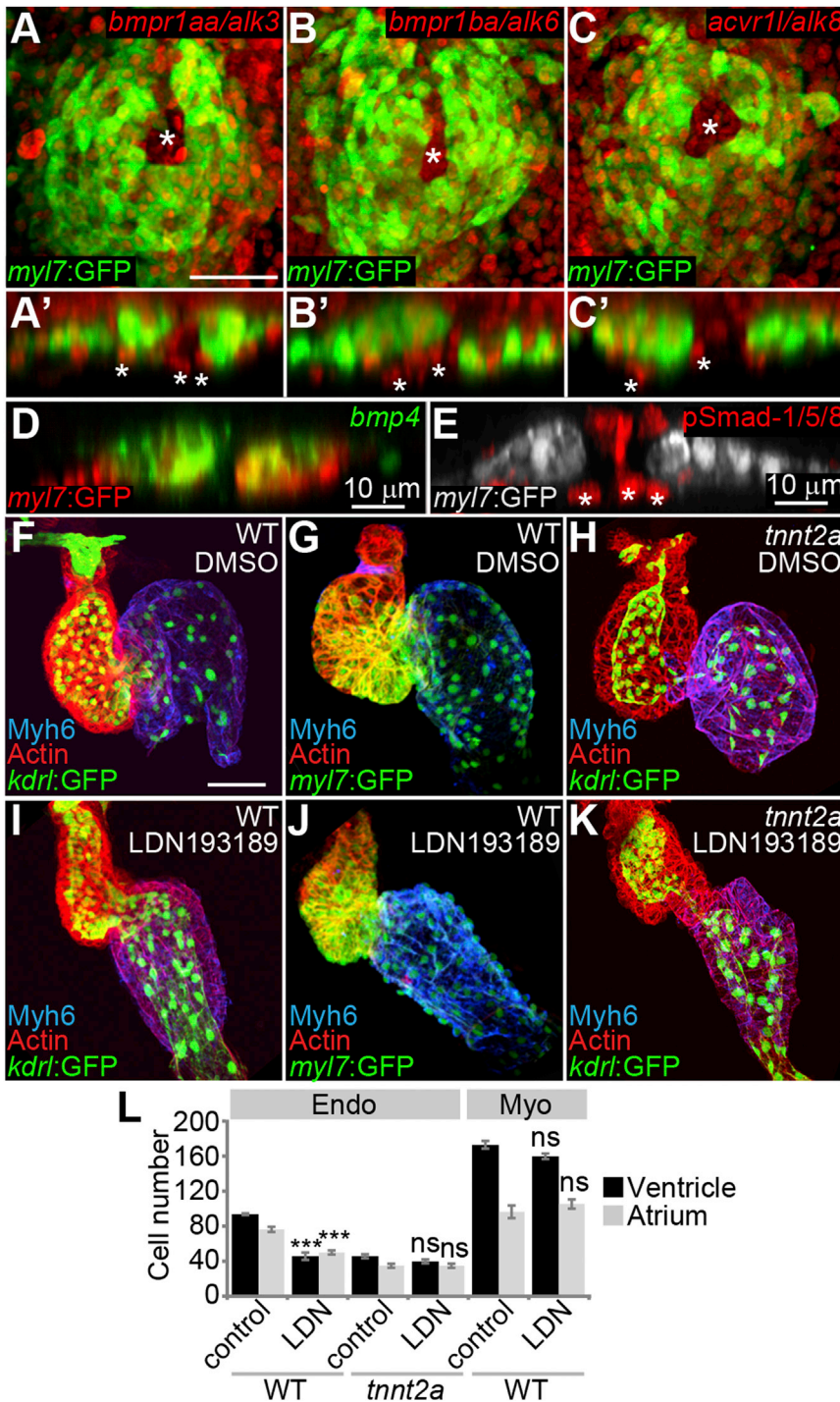
See also Figure S3 and Table S1.

reduced the retrograde flow fraction and shear stress within the heart by targeting only *gata2* (Vermot et al., 2009). Vermot and colleagues measured that the proportion of retrograde flow is lower in *gata2* morphants than in *gata1/2* double morphants while the blood viscosity is reduced by ~70% compared to wild-type (WT; Vermot et al., 2009). Consistent with the study by Vermot and colleagues, we found that *gata2* morphants have a reduced heartbeat rate compared with *gata1/2* double morphants, which is indicative of a lower retrograde flow fraction (Table S1).

In comparison with the differently sized chambers of WT hearts, *tnnt2a*[b109] mutant heart chambers were more similar in size at 54 hpf (Figure 2J). Quantifications of endocardial cell numbers using the endothelial reporter line Tg(*kdrl:EGFP*)[s843] in combination with chamber-specific myocardial markers revealed significantly reduced endocardial cell numbers at 54 hpf in both chambers of the *tnnt2a*[b109] mutant heart compared with WT (Figure 2M), which correlated with a reduced relative proliferation rate between 30 and 54 hpf (Figure 2N). This finding was further confirmed by a short BrdU incubation between 48 and 54 hpf, which indicated a lower rate of proliferative

events compared with WT (Figures S3A, S3B, and S3E). Hence, altered blood flow and/or contractility affects endocardial cell proliferation.

To assess whether the retrograde flow fraction has an effect on endocardial cell number, we analyzed *gata2* morphants that have less shear stress and a reduced retrograde flow fraction compared with *gata1/2* double morphants that have mainly a reduction in shear stress (Figures 2K and 2L; Table S1; Vermot et al., 2009). With this comparison, we could assess the relative effects of altered blood viscosity with that of a changed retrograde flow fraction for endocardial cell numbers. Targeting *gata2* caused a stronger reduction of ventricular endocardial cell numbers (Figure 2M) and a lower relative proliferation rate between 30 and 54 hpf than the knockdown of *gata1/2* (Figure 2N). Hence, the proportion of retrograde flow is a more important hemodynamic parameter for ventricular endocardial cell proliferation than blood viscosity and shear stress. In comparison, targeting *gata2* or both *gata1/2* caused a comparable reduction of atrial endocardial cell numbers (Figure 2M). Similarly, BrdU pulse labeling with a short incubation between 48 and 54 hpf revealed that the number of endocardial cells that

Figure 3. Bmp Signaling within Endocardium Affects Endocardial Cell Numbers during Cardiac Ballooning

(A–E) Endocardial Bmp signaling immediately before cardiac ballooning. (A–C′) Dorsal confocal z-scan projection (A–C) and orthogonal section (A′–C′) views of fluorescence two-color in situ hybridizations in Tg(myl7:EGFP)^{twu34} embryos show the expression of Bmp receptor genes alk3/6/8 within endocardium (white asterisks).

(D) bmp4 is expressed within myocardium as shown with an orthogonal section view in a Tg(myl7:EGFP)^{twu34} embryo (myocardium false-colored in red).

(E) Comparable orthogonal section view shows high pSmad-1/5/8 levels within endocardial progenitor cells (myocardium false-colored in white).

(F–L) Involvement of Bmp signaling in the control of endocardial cell number. (F–H) Hearts treated with 0.2% DMSO (control) or (I–K) 20 μM LDN193189 throughout cardiac ballooning stages (24–54 hpf). (L) Quantifications reveal a strong effect of Bmp inhibition on endocardial but not on myocardial cell numbers (mean with SEM; n ≥ 3 hearts per condition; ns, not significant; ***p < 0.001). Unless otherwise specified, scale bar represents 50 μm.

See also Figure S4.

ventricular endocardium more strongly than shear stress. Thus hemodynamic forces have an impact on endocardial cell numbers (most strongly within the ventricular chamber) and are an important factor during endocardial chamber differentiation.

Bmp Signaling Affects Endocardial Cell Numbers during Cardiac Ballooning

We observed that blood flow had a strong effect also on myocardial chamber dimensions (Figure 2O). Hence, another cue for attuning endocardial proliferation within the growing heart may come from the surrounding myocardium. To further elucidate this possibility, we focused on Bmp signaling since this pathway regulates VEGF-independent angiogenesis in a subset of blood vessels in the developing zebrafish embryo (Wiley et al., 2011; Wiley and Jin, 2011). Several Bmps including Bmp4 are expressed within the heart at the onset of cardiac ballooning stages (Veerkamp et al., 2013). To depict the distribution of Bmp ligand and receptor gene expression within the early zebrafish heart, we performed two-color in situ hybridization experiments for several candidate genes. Several Bmp receptor genes required for Bmp signaling are strongly expressed within the endocardium (Figures 3A–3C), whereas the ligand bmp4 is expressed within the myocardium only (Figure 3D). We next assayed Bmp

had undergone DNA replication was particularly low within the ventricular chamber of gata2 morphants compared with that of gata1/2 double morphants (Figures S3C–S3E). None of the MO injections was associated with increased levels of apoptotic cell death as determined by immunolabeling against caspase-3 (Figures S3F–S3J). This defines the endocardium as a flow-sensitive tissue during cardiac ballooning stages and suggests that the retrograde flow fraction affects proliferation within the

signaling activity at the level of the downstream receptor-regulated- (R-) Smads-1/5/8 that are phosphorylated (pSmad-1/5/8) upon type I and type II Bmp receptor activation. Based on the phosphorylation status and intensity of pSmad-1/5/8, endocardial cells are highly responsive to Bmp signaling at the onset of cardiac ballooning stages (Figure 3E). This endocardial response to Bmp signaling was not dependent on blood flow based on high intensity levels of pSmad-1/5/8 within $tnnt2a^{b109}$ mutant heart chambers (Figure S4). The distribution of Bmp ligand and receptor gene expression combined with a strong Bmp signaling activity within the endocardium was suggestive of Bmp signaling from myocardium toward endocardium.

To inhibit Bmp signaling, we used the small molecule inhibitor LDN193189, which selectively interferes with the Bmp type I Alk2, Alk3, and Alk6 receptors without inhibiting the activation of VEGFR2 (Cannon et al., 2010). Incubation of zebrafish embryos between 24 and 54 hpf with 20 μM of the inhibitor resulted in severely reduced endocardial cell numbers within each chamber at 54 hpf, comparable to a complete loss of blood flow (Figures 3F, 3H, 3I, and 3L). Because the inhibition of Bmp signaling combined with a lack of blood flow did not further reduce endocardial cell numbers at 54 hpf, each condition must already have a severe impact on endocardial cell proliferation (Figures 3K and 3L). In comparison, cardiomyocyte cell numbers of both chambers were unchanged upon pharmacological inhibition of Bmp signaling (Figures 3G, 3J, and 3L). Taken together, these findings identify Bmp signaling as an important regulatory pathway controlling endocardial cell number during cardiac ballooning. Because Bmp signaling is not modulated in response to the mechanical stimulus of blood flow, this is one additional mode by which endocardial cell proliferation is adjusted to the growth of the myocardial chambers.

Endocardial Ballooning Involves Chamber- and Region-Specific Cell Area Size Changes

Whereas the two cardiac chambers contained approximately the same number of endocardial cells, quantitative measurements of chamber volume showed that the atrium is approximately three times larger than the ventricle and the outflow tract region of the ballooning heart at 54 hpf (Figure 4A). We postulated that differences in endocardial cell surface area might be an important factor contributing to the differently sized endocardial chambers that develop during cardiac ballooning. To analyze the impact of cell morphology on endocardial chamber morphogenesis during cardiac ballooning stages, we quantified endocardial cell surface areas between 30 and 54 hpf. Endocardial cell membranes in the transgenic reporter line Tg(kdrl:EGFP)^{s843} were immunolabeled with an antibody against vascular endothelial (VE)-cadherin and, subsequently, endocardial cell surface areas were quantified using the Web-based image tool Image J (NIH). From 30 to 54 hpf, the average atrial endocardial cell surface area increased significantly, whereas ventricular endocardial cells underwent an average reduction of the cell surface area during the same period. By 54 hpf, ventricular endocardial cells had approximately one-third the surface area size of atrial endocardial cells (Figures 4B and 4C).

The ballooning of the myocardium is a process that involves the formation of bean-shaped chambers with distinctly shaped inner and outer curvature regions. Within the ventricle, cardio-myocytes of the outer curvature elongate perpendicular to the arterial-venous axis of the heart, which contributes to the shaping of this chamber. In part, this process is dependent on blood flow through the ventricle (Auman et al., 2007; Lin et al., 2012). Strikingly, we found that endocardial cells of the ventricular chamber showed proportionally similar region-specific differences of cellular morphologies. Cells acquired region-specific cell surface area sizes that are significantly larger in outer-curvature compared with inner-curvature regions of the ballooning ventricle and atrium at 54 hpf (Figure 4D). We also identified domains with small area-sized endocardial cells at the apex regions of the ventricle and atrium (see asterisks in Figure 4B). Taken together, at 54 hpf ventricular and atrial endocardial cells exhibit inner- versus outer-curvature-specific adaptations within the ballooning heart.

During this period, endocardial cells not only underwent chamber-specific changes of cell surface area sizes, but also altered their morphologies in a way that was highly reminiscent of cardiomyocyte morphogenesis: within the ventricular chamber, cardiomyocytes have more cuboidal and compact shapes, compared with the rather squamous and enlarged atrial cardiomyocytes (Figure 4E). Similarly, we found that ventricular endocardial cells displayed stronger VE-cadherin cell junctions labeling, which is indicative of more cuboidal morphologies, compared with weaker VE-cadherin labeling among atrial endocardial cells that have a more squamous appearance (Figure 4F). We conclude that these cell morphology changes are chamber-specific, which generates differently sized endocardial chambers.

Blood Flow Affects Endocardial Cell Area Sizes and Morphology

Because blood flow is an important regulator of endothelial cell morphology, we next assessed whether hemodynamic forces also affect endocardial cell size and shape. First, we analyzed endocardial cell morphology within the ventricular chambers of $tnnt2a^{b109}$ mutant embryos that completely lack blood flow. Measurements of endocardial chamber volume in $tnnt2a^{b109}$ mutants showed that both chambers were almost identical in size (Figure 4G, see also Figure S5A). In general, ventricular endocardial cells had enlarged surface areas (Figures 4G and 4J) and were more circular in these mutants (Figure 4K). The intensity of the VE-cadherin label was comparable in both chambers, suggesting that these cells had similar morphologies (Figure S5B). Second, we targeted gata2 or gata1/2, which caused a similar increase of cell surface area sizes and an enhanced circularity of ventricular endocardial cells (Figures 4H–4K). Hence, shear stress causes a surface area size reduction and contributes to endocardial cell elongation within the ventricular chamber during cardiac ballooning stages. In comparison, both conditions did not significantly affect atrial endocardial cell surface areas (Figure 4J). Also, shear stress had only a mild effect on atrial endocardial cell elongation (Figure 4K).

Due to the impact of hemodynamic forces, mainly shear stress, on ventricular endocardial cell morphology, we targeted the flow-sensitive transcription factor gene klf2a, which is upregulated within blood vessels under shear-stress conditions (Dekker et al., 2002) and also responds to hemodynamic forces within the endocardium during cardiac valve morphogenesis (Vermot et al., 2009). The role of Klf2a during endocardial
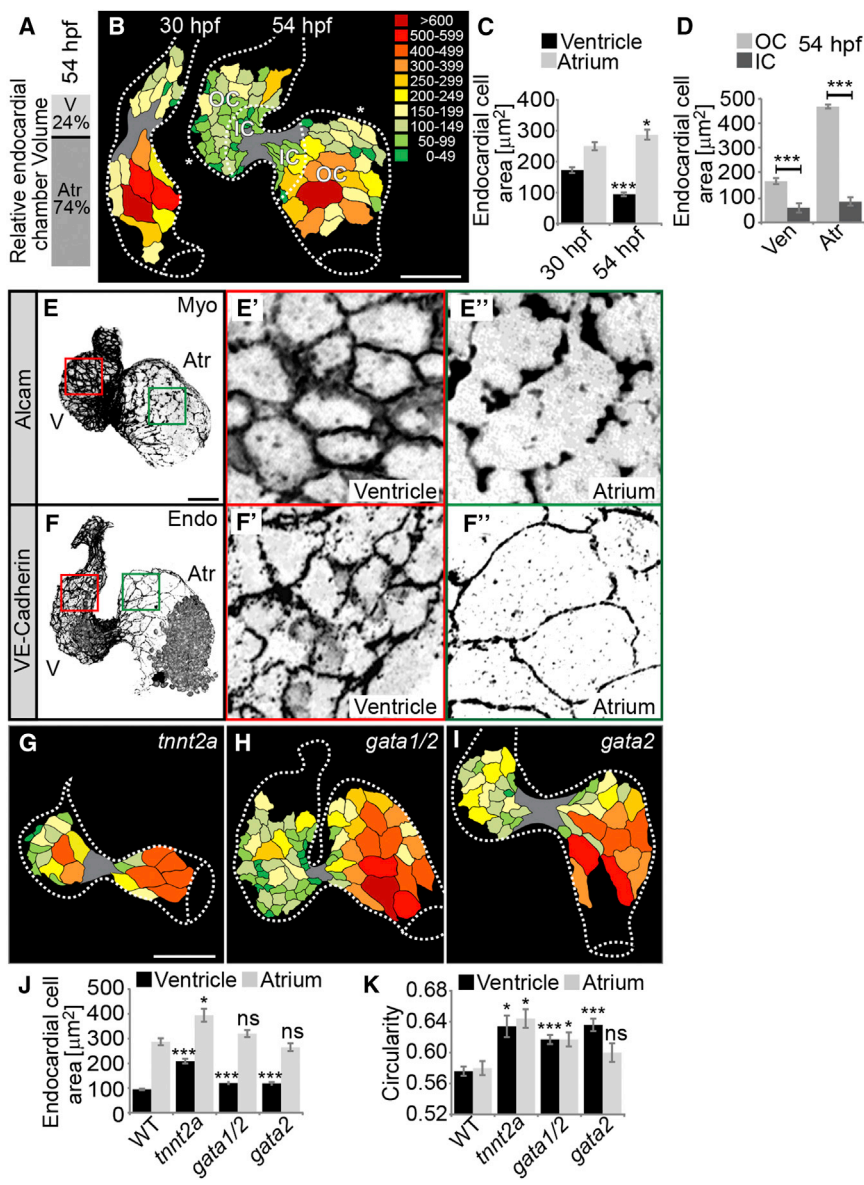
Figure 4. Blood Flow Affects Endocardial Cell Size Changes during Cardiac Ballooning Stages

(A) The atrial chamber volume is about 3-fold larger than that of the ventricle at 54 hpf (volumetric measurements of three hearts).

(B and C) Between 30 and 54 hpf, ventricular endocardial cells decrease in surface area size, whereas atrial endocardial cells increase in surface area size. (B) Both chambers show distinct inner curvature (IC) and outer curvature (OC) regions based on cell surface area size differences (color range indicates area sizes in square micrometers). Asterisks indicate separate apex regions of ventricle and atrium where endocardial cells have small cell surface area sizes. (C) Quantification of average endocardial cell surface area sizes (mean with SEM; n = 8 hearts at 30 hpf and n = 5 hearts at 54 hpf; *p < 0.05; ***p < 0.001).

(D) Endocardial cells of both chambers at 54 hpf have significantly smaller inner curvature cell surface area sizes (mean with SEM; n = 5 hearts; ***p < 0.001).

(E) Chamber-specific differences of myocardial cell morphologies based on Alcam-labeling (inverted image).

(F) Similar chamber-specific differences of endocardial cell morphologies are indicated by differences in VE-cadherin-labeling intensity (inverted image). (E′–F′′) are magnifications of red and green inserts in (E) or (F). (F′′) shows only a single z plane of (F).

(G–I) Hemodynamic forces affect endocardial cell sizes within the ventricle and atrium. Loss of blood flow in $tnnt2a^{b109}$ mutants and reduced shear stress in both $gata1/2$ and $gata2$ morphants causes increased ventricular endocardial cell surface area sizes (same color range as shown in B).

(J and K) Quantifications of average ventricular and atrial endocardial cell surface area sizes and cell circularity show that loss of Tnnt2a or reduced hemodynamic forces cause increased endocardial cell surface area sizes and increased circularity in endocardial cells of both chambers (mean with SEM; n $\geq$ 3 hearts per condition; *p < 0.05; ***p < 0.001). V, ventricle; Atr, atrium. Scale bar represents 50 μm.

See also Figure S5.

chamber morphogenesis had not been addressed prior to this study. The efficiency of the knockdown of $klf2a$ was verified by western blot (Figure 5A), and we found that $klf2a$ morphant embryos had normal cardiac contractility and blood flow (Figure 5B; Table S1; Movies S1 and S2). In the presence of normal hemodynamics, the loss of Klf2a resulted in cell surface area size increases of ventricular endocardial cells, which showed that Klf2a is involved in the blood flow response during endocardial chamber morphogenesis (Figures 5C and 5D). We also observed that altered hemodynamics affected Klf2a levels as assessed by western blot (Figure 5E). To test whether Klf2a is indeed sufficient to restrict endocardial cell surface area size when misexpressed within single endocardial cells, we used a Tg($kdrl:klf2a\_IRES-EGFP$) endothelial promoter expression construct. In line with our hypothesis that Klf2a controls endo-

cardial cellular morphologies in response to blood flow, the overexpression of Klf2a caused a significant decrease in endocardial cell sizes; this effect was most prominent within outer curvature regions of the ventricle, where cells are generally larger (Figures 5F–5H). Hence, blood flow-induced Klf2a plays an important role in restricting endocardial cell area sizes during cardiac ballooning stages. Taken together, our findings show that endocardial cells acquire distinct chamber- and inner- versus outer-curvature-specific area sizes in response to blood flow, which is mediated by the mechanosensitive transcription factor Klf2a.

DISCUSSION

Our work defines the morphogenesis of the endocardial chambers in zebrafish as a process involving cell proliferation and
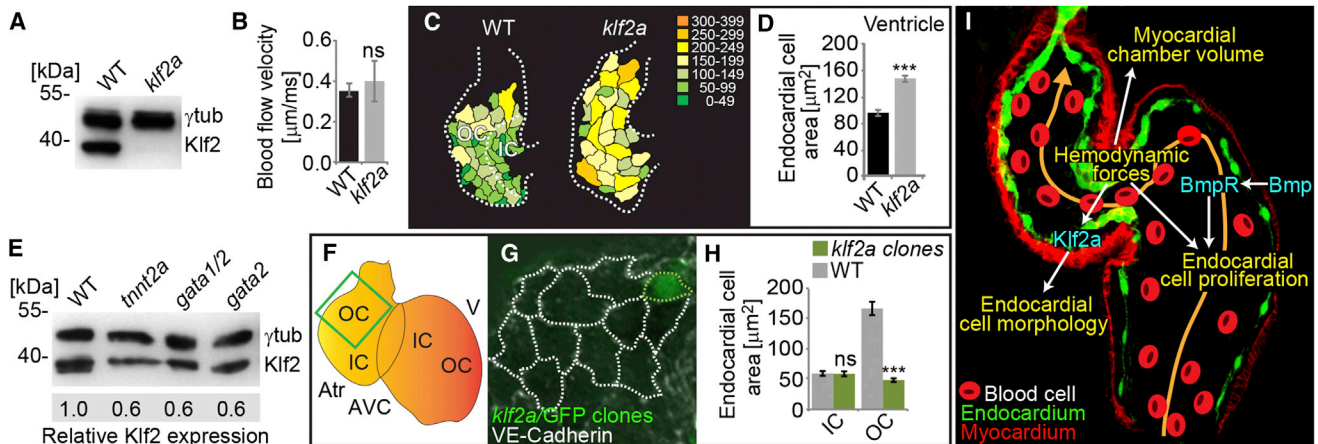
Figure 5. Role of the Mechanosensitive Transcription Factor Klf2a in Endocardial Chamber Morphogenesis

(A) Western blot confirms the efficiency of Klf2a knockdown.

(B) *klf2a* morphant embryos have normal blood flow velocity (mean with SEM based on tracking three blood cells per embryo; n ≥ 3 embryos per condition; ns, not significant).

(C and D) At 54 hpf, loss of Klf2a causes endocardial cell surface area size increases among ventricular endocardial cells (color range is based on area measurements of VE-cadherin-labeled ventricular chambers [in square micrometers]). Inner curvature (IC) and outer curvature (OC) regions are not defined within the *klf2a* morphant ventricular endocardium. (D) Quantifications of average ventricular endocardial cell surface area sizes (mean with SEM; n = 5 ventricular chambers per condition; ***p < 0.001).

(E) Western blot shows lower relative levels of Klf2 under different abnormal hemodynamic conditions at 54 hpf.

(F–H) Endothelial-specific clonal overexpression of Klf2a causes decreased cell surface area sizes. (F) Model of endocardium shows the region (green insert) with the Klf2a overexpression clone shown in (G). (G) Endothelial-specific clonal overexpression of Klf2a (marked with GFP) within the outer curvature causes a decreased cell surface area size. Cell outlines are marked with dotted lines. (H) Quantifications of endocardial cell surface area sizes show that endocardial cells of the outer curvature (OC) expressing Klf2a have the most severe size reduction (mean with SEM; n = 17/17 embryos with such overexpression clones had smaller endocardial cells; ns, not significant; ***p < 0.001).

(I) Model of dynamic crosstalk between endocardium and myocardium during cardiac ballooning morphogenesis. Hemodynamic forces during cardiac ballooning stages control endocardial cell proliferation and, through Klf2a, affect endocardial cell morphology. In addition, hemodynamic forces have an impact on myocardial chamber volume; an effect that is mediated by the endocardium. In turn, Bmp signaling from myocardium may affect endocardial proliferation independently of blood flow. Atr, atrium; V, ventricle; IC, inner curvature; OC, outer curvature. Scale bar represents 50 μm.

See also Movies S1 and S2.

cell surface area changes. During cardiac ballooning, both chambers increase differently in size; we have shown that this differential growth involves endocardial progenitor cell proliferation as well as chamber- and region-specific endocardial cell area size changes. Unlike myocardial chamber ballooning, where an influx of external cells is the major mode of cell number increase (de Pater et al., 2009; Hami et al., 2011; Lazic and Scott, 2011; Zhou et al., 2011), the growth of the endocardial chamber during ballooning stages is primarily due to a chamber-restricted proliferation of endocardial progenitor cells located within the cardiac tube. We have found that this proliferation, during which the number of endocardial cells nearly doubles, is a type of angiogenic growth that requires blood flow but is independent of VEGF signaling. In addition, we have shown that normal proliferation also requires Bmp signaling and that Bmp activity is independent of blood flow. Hence, hemodynamics and Bmp signaling are independent but equally essential contributors to endocardial cell proliferation. We suggest that the early aggregation of endocardium during heart tube assembly stages can be considered as the period of endocardial de novo vasculogenesis, which is followed by a blood flow- and Bmp-dependent form of angiogenic growth during ballooning stages. But similar to the case of myocardial cells, endocardial cells of the ventricle have smaller area sizes and are more cuboidal than those of the

atrium, which contributes to the different sizes of atrial versus ventricular chambers. In addition, endocardial cells of both chambers exhibit inner- versus outer-curvature differences in cell surface area sizes that are similar to the regionally confined cell shape changes observed among myocardial cells of the ventricular chamber (Auman et al., 2007).

Cardiac ballooning involves tightly coupled myocardial and endocardial chamber morphogenesis. The mode of endocardial growth during chamber ballooning suggests that there is some form of coordination between the two cardiac tissues to ensure the proportional increase of endocardial cell number and cell area size relative to the growth of the surrounding myocardium. We have found that region-specific cell surface area size changes during endocardial chamber ballooning are affected by changes in blood flow. A loss of Gata1/2 or of Gata2 severely reduces shear stress within the ballooning zebrafish heart (Vermot et al., 2009), and we found that this caused increased ventricular endocardial cell surface area sizes. Shear stress is a strong inducer of Klf2 (Dekker et al., 2002) and in a manner that parallels reduced shear stress, we found that the targeting of *klf2a* caused an enlargement of endocardial cell surface area sizes within the ventricular chamber. In sum, our data show that the blood flow-responsive transcription factor Klf2a limits endocardial cell size within the ventricle. Vermot and

colleagues showed that the loss of Klf2a directly affects endocardial valve morphogenesis in zebrafish (Vermot et al., 2009). Taken together, this study and ours highlight an important morphogenetic role of Klf2a within endocardium. In a complementary study, Lee and colleagues demonstrated that the loss of Klf2 also has an indirect impact on cardiac form and function due to a changed peripheral tone of the vasculature and increased cardiac output (Lee et al., 2006). Hence, loss of Klf2 can affect cardiac function and development directly due to its role in endocardial morphogenesis and indirectly due to its effect on the peripheral vasculature.

Currently, we can only speculate about the different effects of hemodynamic forces onto the two endocardial chambers. That blood viscosity mainly affects cell surface area and circularity of ventricular endocardial cells indicates that this tissue may be particularly sensitive to this biophysical stimulus or that shear forces are particularly strong within the ventricular chamber. We also found that the retrograde flow fraction is a more important hemodynamic parameter for ventricular endocardial cell proliferation than blood viscosity and shear stress. Whether hematopoietic cells affect endocardial cell proliferation and cell morphology via paracrine signaling still needs to be addressed. However, our findings suggest that the primary effect of hematopoietic cells involves hemodynamics. We found that the severe loss of hematopoietic cells in *gata1/2* double morphants (which should most strongly affect paracrine signaling) has less of an effect on endocardial cell proliferation compared with *gata2* single morphants or *tnnt2a* mutants, which have more hematopoietic cells.

Similarly, blood flow has an instructive role during myocardial chamber ballooning (Auman et al., 2007; Lin et al., 2012), which is most likely mediated by the blood-flow sensitive endocardium. Our work now provides strong additional evidence that the endocardium plays a crucial role as the blood flow-sensitive tissue within the heart during cardiac ballooning stages; this affects not only endocardial proliferation and the control of cell surface area sizes and shapes, but also the proportions of the endocardial chambers and myocardial volume. The instructive role of the endocardium for myocardial chamber morphogenesis is further supported by the observation that increased myocardial ballooning occurs in zebrafish *scl/tal1* mutants, in which endocardial cells fail to associate with the atrial portion of the heart tube, and in *cloche* mutants, which lack endocardium (Bussmann et al., 2007; Holtzman et al., 2007; Schumacher et al., 2013; Stainier et al., 1995).

Conversely, myocardial contractility affects hemodynamics and hence affects endocardial chamber growth. In fact, myocardial chamber differentiation precedes that of the endocardium: chamber-specific expression of myosins and differences of cardiomyocyte morphology are established prior to heart tube formation and before the onset of blood flow (Rohr et al., 2006; Yelon et al., 1999). In contrast, endocardial chamber differentiation is dependent on blood flow, which establishes a chamber-specific expression of genes including *klf2a* and *notch1b* within the ventricular endocardium and at the AVC (Vermot et al., 2009). This temporal sequence of differentiation suggests that first, myocardial chamber-specific actomyosin-dependent contractile properties need to be established; this, in turn, influences chamber-specific hemodynamic forces with an impact on local

klf2a and *notch1b* expression and thus on regional differences in endocardial cell proliferation, morphology, and differentiation. In addition, our work suggests that Bmp signaling from the myocardium is part of a blood flow-independent mechanism by which the proliferation of the endocardium is adjusted to myocardial chamber dimensions.

We have observed chamber-specific differences within the endocardium that involve stronger VE-cadherin junctions labeling and more cuboidal cell morphologies among endocardial cells of the ventricular chamber, which mirror those of ventricular cardiomyocytes. It is plausible that myocardial contractile properties could have an impact on endocardial morphogenesis via distinct processes: A loss of ventricular myosin heavy chain (vmhc) or of cardiac contractility leads to an increase in size of cardiomyocytes and an increased ballooning of the cardiac chambers (Auman et al., 2007), which could have an impact on endocardial cell sizes. It is equally plausible that a reduced blood flow due to the lack of myocardial contractility could more directly affect endocardial and myocardial cell morphologies. In our experiments, a loss of the sarcomeric protein Tnnt2a and a lack of myocardial contractility resulted in lower levels of Klf2a and caused an enlargement of endocardial cells in a manner that is remarkably similar to myocardial cell size increases under this condition. This may explain similarities between region-specific cardiomyocyte and endocardial cell morphologies.

Taken together, our findings are indicative of dynamic interactions between the myocardium and endocardium that constantly attune cellular sizes and shapes, and thus cardiac chamber dimensions in response to physiological changes, the most important of which is blood flow (Figure 5I). Understanding this dynamic crosstalk during development may have implications for understanding how cardiac morphology changes later in life, in response to physiological adaptations or as pathophysiological conditions arise.

EXPERIMENTAL PROCEDURES

Zebrafish Maintenance, Morpholino Injections, Pharmacological Treatment, and Photoconversion Assays

Zebrafish were kept according to standard laboratory procedures (Westerfield, 2007). Handling of zebrafish was done in compliance with German and Berlin state law, carefully monitored by the local authority for animal protection (LaGeSo, Berlin-Brandenburg, Germany). Knockdown studies were performed by MO injection (Gene Tools) as described (Nasevicius and Ekker, 2000). For pharmacological treatments, embryos were incubated in E3 medium containing 5–20 μM Vatalanib (PTK787, Chemie Tek, CT-VT002) or 20 μM LDN193189 (Axon Medchem, Axon 1509) between 24 and 54 hpf. Control embryos were incubated in E3 medium or E3 medium + 0.2% DMSO, respectively. Photoconversion assays were performed as described (Lombardo et al., 2012), with only minor modifications. Homozygous Tg(*kdrl:nlskikGR*)^hsc7 transgenic embryos, which express the photoconvertible fluorescent protein KikGR within endothelial/endocardial cells (Lazic and Scott, 2011), were dechorionated manually at early heart tube stages (27–30 hpf) and embedded in 1% low melting temperature agarose (Lonza, 50081) containing 0.16 mg/ml Tricaine (3-amino benzoic acidethylester; Sigma-Aldrich, A-5040). Embryos were positioned on the left and toward the cover glass to optimize access to the cardiac tube. Prior to photoconversion, KikGR was scanned for green and red fluorescence using the 488 nm argon and the 561 nm DPSS 561-10 lasers, respectively. After photoconversion with a 405 nm diode laser (10% power, 20 iterations), the heart tube was scanned again and documented using the 488 nm and 561 nm lasers. To track

photoconverted endocardial cells at later stages, embryos were removed from the agarose and raised at 28.5°C in egg water until 51–54 hpf. For live imaging, embryos were briefly treated with 40 mM of the myosin ATPase inhibitor BDM (2,3 butanedione monoxime; Sigma-Aldrich, B0753) to suppress the heartbeat and mounted as described above. Due to the changed morphology of the older heart, embryos were embedded with a frontal orientation toward the cover glass to allow imaging of the ballooning heart.

Immunohistochemistry and BrdU Labeling
Immunohistochemical stainings were performed as described (Rohr et al., 2006) with only few modifications (see the Supplemental Experimental Procedures). For BrdU incorporation, Tg(kdrl:EGFP)^{s843} embryos were treated with freshly prepared 5 mg/ml BrdU (Sigma, B5002) in E3 medium between 24 and 48 hpf (long pulse) or between 48 and 54 hpf (short pulse) and processed with mouse anti-BrdU antibody (1:100, Roche,1170376; see the Supplemental Experimental Procedures).

Transient klf2a Misexpression and Plasmids
For misexpression of klf2a within single endocardial cells, Tg(kdrl:Hsa.HRAS-mcherry)^{s896} transgenic embryos were injected at the one-cell stage with a Tg(kdrl:klf2a_IRES-EGFP) misexpression construct (see details of primer design in the Supplemental Experimental Procedures).

Quantification of Cell Parameters and Statistical Analysis
For counting endocardial cells, we used the transgenic endothelial reporter line Tg(kdrl:EGFP)^{s843} (Jin et al., 2005) and both cardiac chambers were identified by counterlabeling the myocardium against Myh6 and rhodamine-phalloidin against actin. AVC cells were recognized based on their characteristic cuboidal morphologies and we confirmed this cell type using a mouse anti-Alcam antibody. This antibody was compatible with other antibodies used for different assays such as rabbit anti-VE-Cadherin (for detailed information about antibodies, see the Supplemental Experimental Procedures). For counting myocardial cells, we used the transgenic myocardial reporter line Tg(myl7:EGFP)^{twu34} (Huang et al., 2003) in combination with anti-Myh6 immunolabeling. Cell numbers and cell area sizes within each chamber were quantified from stacked confocal images using the Web-based image tool Image J (NIH; see the Supplemental Experimental Procedures). For quantification of blood flow velocity, we used the transgenic myeloid linage reporter line Tg(spi1b:Gal4; UAS:EGFP)^{zf149} (Peri and Nüsslein-Volhard, 2008) to track individual cells. Blood flow velocity was calculated in the dorsal aorta (tail region of the embryo) and expressed in micrometers per millisecond (see the Supplemental Experimental Procedures). The p values were obtained by unpaired two-tailed Student's t test.

SUPPLEMENTAL INFORMATION

Supplemental Information includes Supplemental Experimental Procedures, five figures, one table, and two movies and can be found with this article online at http://dx.doi.org/10.1016/j.devcel.2014.06.020.

AUTHOR CONTRIBUTIONS

A.-C.D., V.A.L., J.V., F.P., and S.A.-S. contributed to the conception and design of the experiments. A.-C.D., V.A.L., J.V., and F.P., collected the data. A.-C.D., V.A.L., and S.A.-S. interpreted and analyzed the data. A.-C.D., V.A.L., and S.A.-S. wrote the manuscript and revised the latest version of the manuscript.

ACKNOWLEDGMENTS

REFERENCES

Alt, B., Elsalini, O.A., Schrumpf, P., Haufs, N., Lawson, N.D., Schwabe, G.C., Mundlos, S., Grüters, A., Krude, H., and Rohr, K.B. (2006). Arteries define the position of the thyroid gland during its developmental relocalisation. Development 133, 3797–3804.

Auman, H.J., Coleman, H., Riley, H.E., Olale, F., Tsai, H.J., and Yelon, D. (2007). Functional modulation of cardiac form through regionally confined cell shape changes. PLoS Biol. 5, e53.

Beis, D., Bartman, T., Jin, S.W., Scott, I.C., D'Amico, L.A., Ober, E.A., Verkade, H., Frantsve, J., Field, H.A., Wehman, A., et al. (2005). Genetic and cellular analyses of zebrafish atrioventricular cushion and valve development. Development 132, 4193–4204.

Bussmann, J., Bakkers, J., and Schulte-Merker, S. (2007). Early endocardial morphogenesis requires Scl/Tal1. PLoS Genet. 3, e140.

Cannon, J.E., Upton, P.D., Smith, J.C., and Morrell, N.W. (2010). Intersegmental vessel formation in zebrafish: requirement for VEGF but not BMP signalling revealed by selective and non-selective BMP antagonists. Br. J. Pharmacol. 161, 140–149.

Chan, J., Bayliss, P.E., Wood, J.M., and Roberts, T.M. (2002). Dissection of angiogenic signaling in zebrafish using a chemical genetic approach. Cancer Cell 1, 257–267.

de Pater, E., Clijsters, L., Marques, S.R., Lin, Y.F., Garavito-Aguilar, Z.V., Yelon, D., and Bakkers, J. (2009). Distinct phases of cardiomyocyte differentiation regulate growth of the zebrafish heart. Development 136, 1633–1641.

de Vries, C., Escobedo, J.A., Ueno, H., Houck, K., Ferrara, N., and Williams, L.T. (1992). The fms-like tyrosine kinase, a receptor for vascular endothelial growth factor. Science 255, 989–991.

Dekker, R.J., van Soest, S., Fontijn, R.D., Salamanca, S., de Groot, P.G., VanBavel, E., Pannekoek, H., and Horrevoets, A.J. (2002). Prolonged fluid shear stress induces a distinct set of endothelial cell genes, most specifically lung Krüppel-like factor (KLF2). Blood 100, 1689–1698.

Galloway, J.L., Wingert, R.A., Thisse, C., Thisse, B., and Zon, L.I. (2005). Loss of gata1 but not gata2 converts erythropoiesis to myelopoiesis in zebrafish embryos. Dev. Cell 8, 109–116.

Hami, D., Grimes, A.C., Tsai, H.J., and Kirby, M.L. (2011). Zebrafish cardiac development requires a conserved secondary heart field. Development 138, 2389–2398.

Harris, I.S., and Black, B.L. (2010). Development of the endocardium. Pediatr. Cardiol. 31, 391–399.

Herbert, S.P., and Stainier, D.Y. (2011). Molecular control of endothelial cell behaviour during blood vessel morphogenesis. Nat. Rev. Mol. Cell Biol. 12, 551–564.

Holtzman, N.G., Schoenebeck, J.J., Tsai, H.J., and Yelon, D. (2007). Endocardium is necessary for cardiomyocyte movement during heart tube assembly. Development 134, 2379–2386.

Huang, C.J., Tu, C.T., Hsiao, C.D., Hsieh, F.J., and Tsai, H.J. (2003). Germ-line transmission of a myocardium-specific GFP transgene reveals critical regulatory elements in the cardiac myosin light chain 2 promoter of zebrafish. Dev. Dyn. 228, 30–40.

Jin, S.W., Beis, D., Mitchell, T., Chen, J.N., and Stainier, D.Y. (2005). Cellular and molecular analyses of vascular tube and lumen formation in zebrafish. Development 132, 5199–5209.

Kim, J.D., Kang, H., Larrivée, B., Lee, M.Y., Mettlen, M., Schmid, S.L., Roman, B.L., Qyang, Y., Eichmann, A., and Jin, S.W. (2012). Context-dependent

proangiogenic function of bone morphogenetic protein signaling is mediated by disabled homolog 2. Dev. Cell 23, 441–448.

Lazic, S., and Scott, I.C. (2011). Mef2cb regulates late myocardial cell addition from a second heart field-like population of progenitors in zebrafish. Dev. Biol. 354, 123–133.

Lee, J.S., Yu, Q., Shin, J.T., Sebzda, E., Bertozzi, C., Chen, M., Mericko, P., Stadtfeld, M., Zhou, D., Cheng, L., et al. (2006). Klf2 is an essential regulator of vascular hemodynamic forces in vivo. Dev. Cell 11, 845–857.

Lin, Y.F., Swinburne, I., and Yelon, D. (2012). Multiple influences of blood flow on cardiomyocyte hypertrophy in the embryonic zebrafish heart. Dev. Biol. 362, 242–253.

Lombardo, V.A., Sporbert, A., and Abdelilah-Seyfried, S. (2012). Cell tracking using photoconvertible proteins during zebrafish development. J. Vis. Exp. (67)

Nasevicius, A., and Ekker, S.C. (2000). Effective targeted gene 'knockdown' in zebrafish. Nat. Genet. 26, 216–220.

Nicoli, S., Standley, C., Walker, P., Hurlstone, A., Fogarty, K.E., and Lawson, N.D. (2010). MicroRNA-mediated integration of haemodynamics and VEGF signalling during angiogenesis. Nature 464, 1196–1200.

Olsson, A.K., Dimberg, A., Kreuger, J., and Claesson-Welsh, L. (2006). VEGF receptor signalling - in control of vascular function. Nat. Rev. Mol. Cell Biol. 7, 359–371.

Peri, F., and Nüsslein-Volhard, C. (2008). Live imaging of neuronal degradation by microglia reveals a role for v0-ATPase a1 in phagosomal fusion in vivo. Cell 133, 916–927.

Puri, M.C., Partanen, J., Rossant, J., and Bernstein, A. (1999). Interaction of the TEK and TIE receptor tyrosine kinases during cardiovascular development. Development 126, 4569–4580.

Rohr, S., Bit-Avragim, N., and Abdelilah-Seyfried, S. (2006). Heart and soul/PRKCi and nagie oko/Mpp5 regulate myocardial coherence and remodeling during cardiac morphogenesis. Development 133, 107–115.

Schumacher, J.A., Bloomekatz, J., Garavito-Aguilar, Z.V., and Yelon, D. (2013). tal1 Regulates the formation of intercellular junctions and the maintenance of identity in the endocardium. Dev. Biol. 383, 214–226.

Sehnert, A.J., Huq, A., Weinstein, B.M., Walker, C., Fishman, M., and Stainier, D.Y. (2002). Cardiac troponin T is essential in sarcomere assembly and cardiac contractility. Nat. Genet. 31, 106–110.

Shibuya, M., and Claesson-Welsh, L. (2006). Signal transduction by VEGF receptors in regulation of angiogenesis and lymphangiogenesis. Exp. Cell Res. 312, 549–560.

Stainier, D.Y., Weinstein, B.M., Detrich, H.W., 3rd, Zon, L.I., and Fishman, M.C. (1995). Cloche, an early acting zebrafish gene, is required by both the endothelial and hematopoietic lineages. Development 121, 3141–3150.

Staudt, D., and Stainier, D. (2012). Uncovering the molecular and cellular mechanisms of heart development using the zebrafish. Annu. Rev. Genet. 46, 397–418.

Veerkamp, J., Rudolph, F., Cseresnyes, Z., Priller, F., Otten, C., Renz, M., Schaefer, L., and Abdelilah-Seyfried, S. (2013). Unilateral dampening of Bmp activity by nodal generates cardiac left-right asymmetry. Dev. Cell 24, 660–667.

Vermot, J., Forouhar, A.S., Liebling, M., Wu, D., Plummer, D., Gharib, M., and Fraser, S.E. (2009). Reversing blood flows act through klf2a to ensure normal valvulogenesis in the developing heart. PLoS Biol. 7, e1000246.

Westerfield, M. (2007). The Zebrafish Book: A Guide for the Laboratory Use of Zebrafish (Danio rerio), Fourth Edition. (Eugene: University of Oregon Press).

Wiley, D.M., and Jin, S.W. (2011). Bone morphogenetic protein functions as a context-dependent angiogenic cue in vertebrates. Semin. Cell Dev. Biol. 22, 1012–1018.

Wiley, D.M., Kim, J.D., Hao, J., Hong, C.C., Bautch, V.L., and Jin, S.W. (2011). Distinct signalling pathways regulate sprouting angiogenesis from the dorsal aorta and the axial vein. Nat. Cell Biol. 13, 686–692.

Yelon, D., Horne, S.A., and Stainier, D.Y. (1999). Restricted expression of cardiac myosin genes reveals regulated aspects of heart tube assembly in zebrafish. Dev. Biol. 214, 23–37.

Zhou, Y., Cashman, T.J., Nevis, K.R., Obregon, P., Carney, S.A., Liu, Y., Gu, A., Mosimann, C., Sondalle, S., Peterson, R.E., et al. (2011). Latent TGF-β binding protein 3 identifies a second heart field in zebrafish. Nature 474, 645–648.